

Higher Order HTSC Gradiometer for Measurements in Unshielded Environment

P. Seidel, C. Becker, A. Steppke, U. Schinkel, K. Hofer, V. Grosse, S. Engmann, F. Schmidl, and L. Redlich

Abstract— We present a new higher order gradiometer layout for bicrystal Josephson junctions based on high-temperature superconducting thin films. Our single layer gradiometers are suitable for the simultaneous measurement of magnetic field gradients with different spatial orientations. The sophisticated technology for bicrystal Josephson junctions is combined with custom substrates with two crossing 30 degree grain boundaries. We present the technological challenges focusing on the low ohmic contact resistance using gold nanoparticles embedded in the thin film. The sensor performance is characterized using SQUID electronics. Its main parameters such as critical current and $I_C R_N$ -product are compared with parameters of first order gradiometers on single 30 degree bicrystal substrates. Special emphasis is put on the optimization of the noise properties in unshielded environment.

Index Terms—Antennas, Josephson junction, magnetic field measurement, noise, SQUIDs

I. INTRODUCTION

FOR the measurement of small magnetic fields, superconducting quantum interference devices, so called DC-SQUIDS are the most sensitive sensors. They are applied in various research areas, e.g., biomagnetism, geophysical exploration and nondestructive evaluation [1-4].

The application of high- T_C superconductors produces lower costs by cooling with liquid nitrogen or a small non-magnetic refrigerator [5]. With silicon dioxide passivation the sensors can be made with long-term stability of their electrical properties thus extending their application areas [6].

In many cases the spatial distribution of the magnetic field contains important information. Hence, in such systems several DC-SQUID gradiometers measure the orthogonal components of the magnetic field gradient [7,8]. We transferred this concept established in low- T_C applications on

the high- T_C superconductor $YBa_2Cu_3O_{7-x}$ (YBCO) and created a new gradiometer layout for the simultaneous measurement of the coplanar orthogonal field gradients on a single 10×10 mm² substrate [9]. To permit a wide area of application the sensor should be operational in a magnetically unshielded environment. Therefore, the sensors are analyzed within this paper with respect to their voltage modulation and noise characteristics.

II. SENSOR CONCEPT

Starting point for the new layout is a direct coupled planar DC-SQUID gradiometer, which allows the measurement of the flux differences along the gradiometer axis. Since the SQUID loop inductance is negligible compared to the antenna inductance L_{Ant} the difference of the antenna currents $I_{Ant/1}$ and $I_{Ant/2}$ is given by

$$\Delta I_{Ant} = I_{Ant/1} - I_{Ant/2} = \frac{\Delta B \cdot A_{Ant}}{L_{Ant}}, \quad (1)$$

where ΔB and A_{Ant} are the difference of the magnetic fields and the antenna area, respectively. This differential current is detected by a galvanically coupled DC-SQUID. Thus, the DC-SQUID works as a current-flux-voltage-converter. The variation of the voltage ΔV_{SQUID} within the DC-SQUID can be characterized by following equation

$$\begin{aligned} \Delta V_{SQUID} &= V_\phi \cdot \Delta \phi_{SQUID} = V_\phi \cdot L_{SQUID} \cdot \Delta I_{Ant} \\ &= V_\phi \cdot L_{SQUID} \cdot \frac{\Delta B \cdot A_{Ant}}{L_{Ant}} = V_\phi \cdot \Delta B \cdot A_{eff}. \end{aligned} \quad (2)$$

Here V_ϕ is the transfer function and L_{SQUID} is the mutual inductance.

By arranging two planar gradiometers orthogonal in the x-y-plane, the magnetic field gradient $\Delta B_z / \Delta x$ and $\Delta B_z / \Delta y$ can be measured. For an accurate measurement of the field gradients with a high resolution the two gradiometers were unified. With the new layout shown in Fig. 1 we are able to measure four independent field gradients with four coupled gradiometers. Furthermore, the second order field gradient $\Delta^2 B_z / (\Delta x \Delta y)$ in the diagonal direction can be determined via a suitable software evaluation. For this the signals of the DC-SQUID SQ1 (or SQ3) and neighboring SQ2 (or SQ4) have to be recorded.

Manuscript received 15 August 2008. This work was supported in part by the project EU BIODIAGNOSTICS (017002).

P. Seidel, C. Becker, U. Schinkel, K. Hofer, V. Grosse, S. Engmann and F. Schmidl are with the Institut für Festkörperphysik, Friedrich-Schiller-Universität Jena, D-07743 Jena, Germany (phone: +49-3641-947410; fax: +49-3641-947412; e-mail: Paul.Seidel@uni-jena.de).

A. Steppke, was with Institut für Festkörperphysik, Friedrich-Schiller-Universität Jena, D-07743 Jena, Germany. He is now with the Max-Planck-Institut für Chemische Physik fester Stoffe, D-01187 Dresden, Germany (e-mail: Alexander.Steppke@cpfs.mpg.de).

L. Redlich is with the Institut für Photonische Technologien, D-07745 Jena, Germany (e-mail: lutz.redlich@iphht-jena.de).

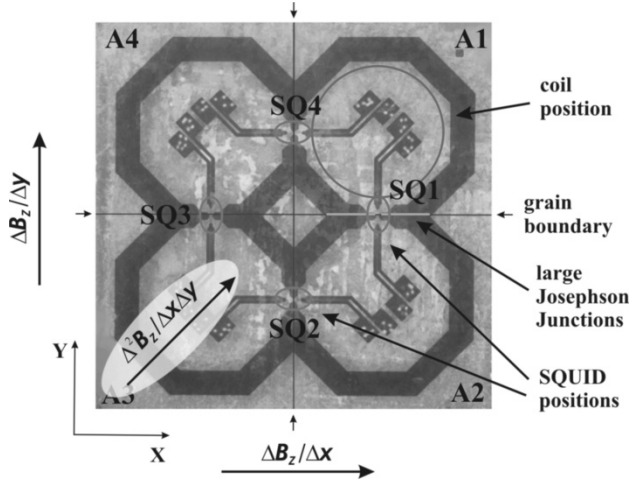


Fig. 1. The photograph shows the fabricated gradiometer. The positions of the DC-SQUIDS are marked with SQ1-SQ4 and the antennas are marked with A1-A4. The crossed bicrystal substrate has a size of $10 \times 10 \text{ mm}^2$.

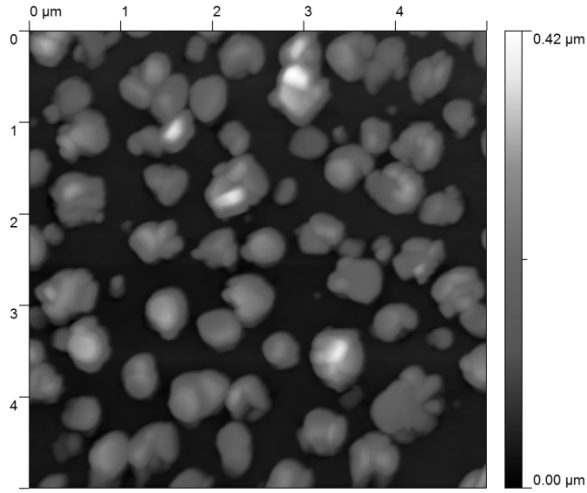


Fig. 2. AFM topographic image showing Au cluster embedded in an YBCO thin film on a STO substrate which forms the contact area. For the preparation see the section III in this paper.

III. SENSOR PREPARATION

We used SrTiO_3 crossed bicrystal substrates with symmetric 30° grain boundaries to allow an orthogonal arrangement of the gradiometers [9]. YBCO thin films with thicknesses of 150 nm were grown by pulsed laser deposition at 1100 K in a 50 Pa oxygen atmosphere [10]. The films were proved to be c-oriented with rocking-curve widths of $<0.3^\circ$ and critical current densities $>2 \times 10^6 \text{ A/cm}^2$.

To obtain a low contact resistance between the superconducting film and the bonding wire, a technique first presented in Seidel et al. [6] was further enhanced to reduce negative effects on the YBCO properties. Before the YBCO deposition, we grew a 20 nm thick gold layer in the area of the bonding pad. The gold layer reorganizes to clusters with diameters in the range between 300 to 600 nm, while the YBCO layer grows nearly unaffected. The resulting films showed no measurable degradation in T_C or the critical current density. Moreover, we found a local reduction in the rocking-curve width in regions with gold particles compared to those without gold particles.

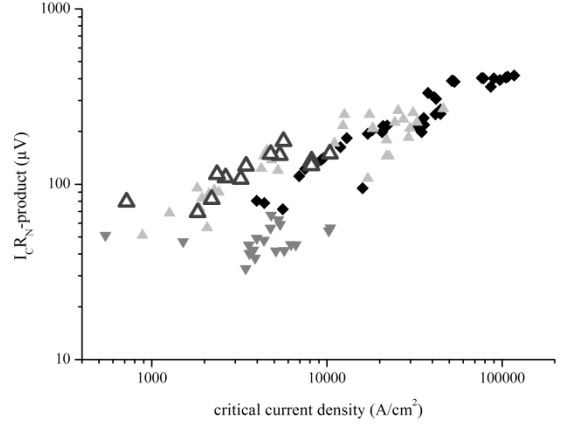


Fig. 3. $I_C R_N$ -product of bicrystal Josephson junctions as a function of the critical current density J_C . Symbols (\blacklozenge) 24° , (\blacktriangle) 30° and (\blacktriangledown) 36° are single bicrystals STO substrates. The open triangular symbols are the measured SQUIDS on crossed bicrystals used for the new gradiometer.

Due to a lateral misalignment of two grain boundaries in the crossed bicrystal substrate two exposure steps during the photolithography process are necessary. After the creation of the antenna structure each of the four DC-SQUID structures is aligned individually to the grain boundaries [9]. The structure was etched utilizing argon ion beam etching. To prevent heating and thus degradation of the YBCO layer, the sample was placed on a cold finger sample holder cooled by liquid nitrogen.

The gradiometer antenna inductance in our layout amounts to 4.85 nH, while the effective antenna area is $0.141 \pm 0.005 \text{ mm}^2$. The mutual inductance of a single DC-SQUID is 49 pH and the DC-SQUID having a loop length of 40 μm and a loop width of 5 μm . The Josephson junction width is 3 μm with critical currents between 20-50 μA .

IV. EXPERIMENTAL RESULTS

A. Noise properties of the 30° grain boundaries

The $I_C R_N$ -product of our new layout lies in the same range as previously measured gradiometers on single bicrystal substrates with a 30° grain boundary, see Fig. 3. Thus, it appears that the use of crossed bicrystals shows no significant effect in comparison to single bicrystals. Generally, the $I_C R_N$ -product for 30° grain boundaries is reduced compared to that for 24° grain boundaries. This results in a smaller transfer function. Additionally, the voltage noise of the DC-SQUIDS depends on the critical current [11]. This results in a complicated dependence of the noise properties on different angles of the grain boundary. If $\sqrt{S_V}$ presents the voltage noise and $\sqrt{S_\phi}$ is the flux noise of the device, then the field gradient noise $\sqrt{S_G}$ is described by

$$\sqrt{S_G} = \frac{\sqrt{S_\phi}}{b \cdot A_{\text{eff}}} = \frac{\sqrt{S_V}}{b \cdot A_{\text{eff}} \cdot V_\phi}, \quad (3)$$

where b is the baseline length of the gradiometer and A_{eff} is the effective area.

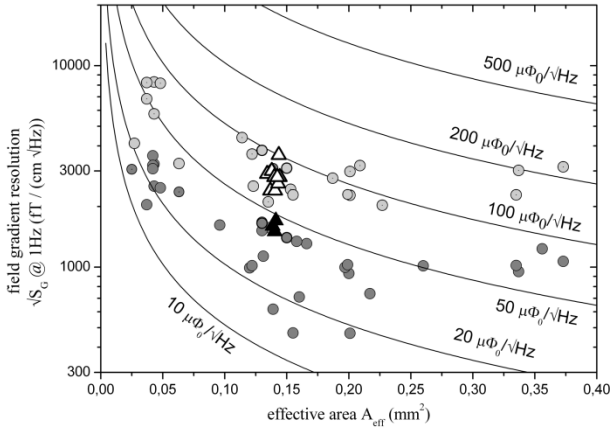


Fig. 4. Field gradient resolution $\sqrt{S_G}$ versus the effective area of the gradiometer. The triangular symbols (\blacktriangle) are the measured SQUID gradiometers on crossed bicrystals. Measurements in unshielded environment are marked with open symbols. The circular symbols represent the data of gradiometers on single bicrystal substrates with different grain boundary angles in shielded (dark grey) and unshielded (light grey) environment [11].

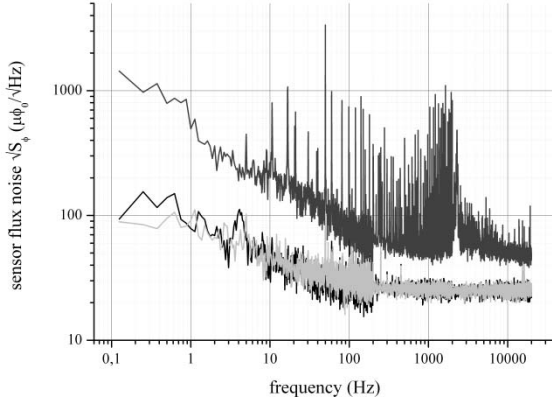


Fig. 5. Sensor flux noise for unshielded environment (grey), with a single μ -metal shields (light grey) and two μ -metal shields (black).

To evaluate the noise properties of the new gradiometer layout on 30° crossed bicrystal substrates we plotted the field gradient noise at 1 Hz in comparison with the data of previously measured gradiometers on single bicrystal substrates, see Fig. 4. The value of the $1/f$ noise at 1 Hz remains in the upper limit of all other gradiometers [11,12]. This indicates that the new layout exhibits no additional noise sources compared to our previous layouts. We also determined the values for unshielded measurements to be in the range of the comparison specimen. Fig. 5 shows the flux noise properties of the new gradiometer. In a magnetically unshielded environment the noise level increased by a factor of 8 compared to a single and double μ -metal shielding.

B. Voltage modulation anomaly

To evaluate how an unshielded environment affects the functionality of the sensor we measured the voltage modulation of the DC-SQUID SQ1 at small fields generated with a coil placed under antenna A2. The results in the earth's magnetic field are illustrated in Fig. 6. Abnormal field dependences are observed.

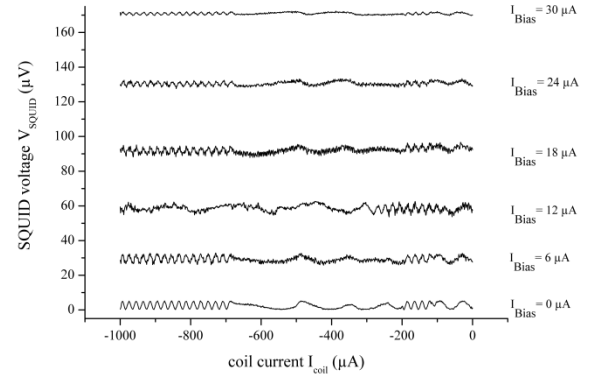


Fig. 6. Voltage modulation anomaly of the SQUID in external magnetic field measured for different bias currents I_{Bias} .

The current in the coil which induces the external magnetic field was swept from -1 mA to 0 mA. In the range from -1 mA to -0.7 mA a normal voltage modulation was observed. However, between -0.7 mA and -0.2 mA the modulation disappears, to be recovered again in the range from -0.2 mA to -0.1 mA.

The origin of this effect lies in the grain boundaries crossing the antenna structure, see Fig. 1. As the 30° grain boundary contacts have a reduced current density, we analyzed the parameter critical current in this area. The contact width of these large Josephson junctions $w_{largeJJ}$ amounts to 1256 μm .

TABLE 1 Important Sensor Characteristics

Sensor value	Experimental results
$I_{C\ SQUID}$	(10-50) μA
$J_{C\ thin\ film}$	(2.0-2.7) $\times 10^6$ A/cm ²
$J_{C\ JJ}$	(2.2-11.0) $\times 10^3$ A/cm ²
$J_{C\ Large\ JJ}$	(1.20 \pm 0.02) $\times 10^3$ A/cm ²
L_{Ant}	(4.85 \pm 0.15) nH
L_{SQUID}	(49 \pm 2) pH
$B_{C\ Ant}$	(0.80 \pm 0.01) μT
A_{eff}	(0,141 \pm 0.005) mm ²

The current-voltage characteristics of the large junctions were measured by a four point contact method. For that purpose we cut one side of the antenna structure and separated the SQUID from this part. As result we get a single large Josephson junction. The critical current density was determined to (1.20 \pm 0.02) $\times 10^3$ A/cm². Furthermore, the influence of an external homogeneous magnetic field perpendicular to the grain boundary was investigated. The results are illustrated in Fig. 7. Strong linear decreases of I_C with an increasing external magnetic field were observed, indicating a typical behavior of a large Josephson junction [13-18]. We calculated the ratio of the junction width w and the Josephson penetration length λ_J to be $w/\lambda_J \sim 100$.

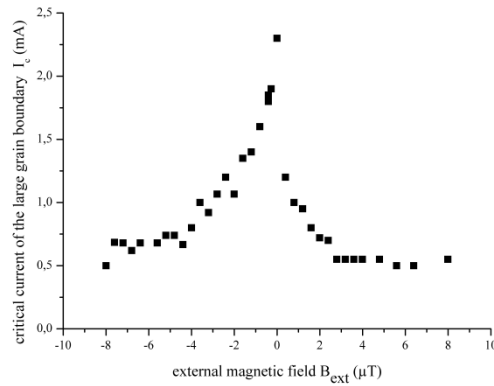


Fig. 7. Critical current vs. external magnetic field of a large Josephson junction with $w/\lambda_J \sim 100$, which occurs as a parasitic junction within the antenna loop.

The voltage modulation of a DC-SQUID depends on the incoupling current through the SQUID loop. For an ordinary gradiometer on a single bicrystal substrate this current is identical to the difference in the two antenna screening currents I_{Ant1} and I_{Ant2} . However, our new layout provides several paths in the whole antenna structure for a circulating screening current. So the incoupling current in a single DC-SQUID is influenced by the total distribution of the screening current in the gradiometer structure.

As shown in Fig. 7 an external magnetic field reduces the critical current of a large Josephson junction formed by the grain boundary crossing the antenna. If the screening current exceeds the critical current of this junction it gets resistive. This leads to a redistribution of the screening currents and therewith the incoupling currents through the SQUID loop. This results in an abnormal voltage modulation depending on the coil current.

V. CONCLUSION

We measured the new gradiometer fabricated on 30° crossed grain boundary substrates in an external magnetic field B_{ext} , and in particular its noise properties. The $I_c R_N$ -product and the field gradient noise turned out to be comparable with gradiometers on single bicrystal substrates. In certain external magnetic fields the voltage modulation displays abnormal behavior. A possible explanation for this effect is a redistribution of the screening current in the antenna structure caused by large Josephson junctions.

Further measurements of all large junctions in the gradiometer and simulations of the gradiometer structure have to be performed to verify this conclusion and to prove our assumption. The layout will be improved to increase the critical current either by increasing the line width across the grain boundary or the film thickness. Additionally, the grain boundaries through the antenna structure could be prevented by employing step edge Josephson junctions for the fabrication of the SQUID loops.

REFERENCES

- [1] I.-S. Kim, K. K. Yu, Y. H. Lee, K. W. Kim, and Y. K. Park, "High- T_C SQUID Magnetometers for Low Noise Measurements of Magnetocardiograms," *IEEE Trans. Appl. Supercond.*, vol. 15, pp. 652-655, 2005.
- [2] H.-C. Yang, T.-Y. Wu, H.-E. Horng, C.-C. Wu, S. Y. Yang, S.-H. Liao, C.-H. Wu, J. T. Jeng, J. C. Chen, K.-L. Chen, and M. J. Chen, "Scanning high- T_C SQUID imaging system for magnetocardiography," *Supercond. Sci. Technol.*, vol. 19, pp. 297-302, 2006.
- [3] H.-G. Meyer, R. Stolz, A. Chwala, and M. Schulz, "SQUID technology for geophysical exploration," *Phys. Stat. Sol.*, vol. 2, pp. 1504-1509, 2005.
- [4] S. Wunderlich, F. Schmidl, H. Specht, L. Doerrer, H. Schneidewind, U. Hueber, and P. Seidel, "Planar gradiometers with high- T_C DC SQUIDs for non-destructive testing," *Supercond. Sci. Technol.*, vol. 11, pp. 315-321, 1998.
- [5] C. Becker, A. Steppke, T. Koettig, J. Gerster, L. Dörrer, M. Thürk, F. Schmidl, and P. Seidel, "Operation of a high- T_C DC-SQUID-gradiometer on a non-metallic pulse tube refrigerator," *Journal of Physics: Conf. Series*, vol. 97, pp. 1-6, 2008.
- [6] P. Seidel, C. Becker, A. Steppke, M. Buettner, H. Schneidewind, V. Grosse, G. Zieger, and F. Schmidl, "Long-time stable high-temperature superconducting DC-SQUID gradiometers with silicon dioxide passivation for measurements with superconducting flux transformers," *Supercond. Sci. Technol.*, vol. 20, pp. 380-384, 2007.
- [7] Y. Adachi, J. Kawai, M. Miyamoto, G. Uehara, S. Kawabata, H. Okubo, Y. Fukuoka, and H. Komori, "Three dimensionally configured SQUID vector gradiometers for biomagnetic measurement," *Supercond. Sci. Technol.*, vol. 16, pp. 1442-1446, 2003.
- [8] G. Kallias, E. Devlin, C. Christides, and D. Niarchos, "High T_C squid sensor system for non-destructive evaluation," *Sens. Actuators*, vol. 85, pp. 239-243, 2000.
- [9] A. Steppke, C. Becker, V. Grosse, L. Dörrer, F. Schmidl, P. Seidel, M. Djupmyr, and J. Albrecht, "Planar high- T_C superconducting quantum interference device gradiometer for simultaneous measurements of two magnetic field gradients," *Appl. Phys. Lett.*, vol. 92, pp. 1122504-1-122504-3, 2008.
- [10] P. Seidel, F. Schmidl, H. Wald, M. Mans, K. Peiselt, U. Baldeweg, M. Beck, S. Biering, C. Becker, J. Uhlig, and V. Große, "Thin-Film Technology for HTSC Josephson Devices," *IEEE Trans. Appl. Supercond.*, vol. 15, pp. 161-164, 2005.
- [11] P. Seidel, C. Becker, A. Steppke, T. Foerster, S. Wunderlich, V. Grosse, R. Pietzcker, and F. Schmidl, "Noise properties of high-temperature superconducting dc-SQUID gradiometers," *Physica C*, pp. 331-334, 2007.
- [12] P. Seidel, T. Foerster, H. Schneidewind, C. Becker, V. Grosse, A. Steppke, P. Lorenz, R. Peitzcker, and F. Schmidl, "Comparison of High Temperature Superconducting Gradiometers Using Flip Chip YBCO and TBCCO Antennas," *IEEE Trans. Appl. Supercond.*, vol. 17, pp. 668-671, 2007.
- [13] A. Barone, G. Paterno, *Physics and Application of the Josephson Effect*. New York: Wiley, 1982, ch. 5.
- [14] Y. Enomoto, Z. Hao, S. Hirano, and K. Suzuki, "Characteristics of Long Grain Boundary Josephson Junctions on Bicrystal Substrates," *Jpn. J. Appl. Phys.*, vol. 41, pp. L925-L927, 2002.
- [15] K. Lee, and I. Iguchi, "Josephson effects in $YBa_2Cu_3O_y$ grain boundary junctions on (100)MgO bicrystal substrates," *Appl. Phys. Lett.*, vol. 66, pp. 769-771, 1995.
- [16] C. Weber, A. M. Klushin, M. Darula, R. Semerad, W. Prusseit, and H. Kohlstedt, "Large Shapiro steps and wide junction behaviour in HTS Josephson junctions at nitrogen temperatures," *App. Supercond.*, vol. 5, pp. 451-456, 1998.
- [17] A. M. Klushin, C. Weber, M. Darula, R. Semerad, W. Prusseit, H. Kohlstedt, and A. I. Braginski, "Large critical currents and current steps in shunted bicrystal Josephson junctions at liquid nitrogen temperatures," *Supercond. Sci. Technol.*, vol. 11, pp. 609-613, 1998.
- [18] F. Tafuri, and J. R. Kirtley, "Weak links in high critical temperature superconductors," *Rep. Prog. Phys.*, vol. 68, pp. 2573-2663, 2005.